Dynamics of Subpicosecond Relativistic Laser Pulse Self-Channeling in an Underdense Preformed Plasma

J. Fuchs,[1,2] G. Malka,[3] J. C. Adam,[4] F. Amiranoff,[2] S. D. Baton,[2] N. Blanchot,[3] A. Héron,[4]
G. Laval,[4] J. L. Miquel,[3] P. Mora,[4] H. Pépin,[1] and C. Rousseaux[3]
[1]*Institut National de la Recherche Scientifique—Énergie et Matériaux, 1650 bd. L. Boulet, J3X1S2 Varennes, Québec, Canada*
[2]*Laboratoire pour l'Utilisation des Lasers Intenses, Centre National de la Recherche Scientifique, École Polytechnique, 91128 Palaiseau Cedex, France*
[3]*Commissariat à l'Énergie Atomique, Limeil-Valenton, 94195 Villeneuve-Saint-Georges Cedex, France*
[4]*Centre de Physique Théorique, Centre National de la Recherche Scientifique, École Polytechnique, 91128 Palaiseau Cedex, France*
(Received 28 April 1997)

The formation and evolution of density channels created by the interaction of a short bright (600 fs, 5×10^{18} W cm^{-2} μm^2) laser pulse with a preformed plasma are studied by means of experiments and 2D particle-in-cell (PIC) simulations. Hollow density channels are observed by interferometry, and a fast radial expansion (5×10^8 cm/s) is measured. Magnetic fields around 50 MG inferred from Faraday rotation measurements suggest the occurrence of self-focusing. The PIC simulations support this hypothesis and show ion depletion during the laser pulse as well as radial expansion in agreement with experiments. [S0031-9007(98)05299-5]

PACS numbers: 52.40.Nk, 52.25.Rv, 52.50.Jm, 52.70.Kz

With the progress of compact short-pulse multiterawatt laser systems [1], it has become possible to explore the domain of relativistic laser pulse propagation and channel formation in an underdense plasma. These are topics of considerable interest for the fast ignitor (FI) concept [2], relevant to the inertial confinement fusion (ICF) studies. Indeed, the ultimate interest of this concept relies on the penetration of a short and bright laser pulse in the overdense core and the generation of the electrons that will ignite the fuel. However, to cross the underdense corona without energy losses, this pulse is planned to propagate into a hollow channel. Channel formation has been observed for several years with subrelativistic laser pulses [3]. Density depression in the channel and density increase on its walls are caused by the combined effects of transverse ponderomotive force, space-charge fields, and plasma heating. The channel formation process can be enhanced [4] by the cumulative effects of ponderomotive and relativistic self-focusing [5] which increase drastically the laser intensity, as shown recently in 3D simulations [6]. Moreover, the evacuated channel can act as a beam self-propagation guide, as seen recently [7].

In this Letter, we present direct measurements and 2D particle-in-cell (PIC) simulations that show the dynamics of subpicosecond relativistic laser pulse self-channeling in a fully ionized underdense plasma in the presence of a density gradient. The PIC simulations quantitatively reproduce the experimental results at early and long times. Therefore we rely on the PIC simulation to describe the channel formation during the laser pulse since this is not directly accessible by interferometry. These results are complementary to the ones of Borghesi *et al.* [7] as we put in evidence (i) the local dynamics of channel formation (ion depletion during the laser pulse), (ii) the local dynamics of channel evolution (radial expansion of the channel after the laser pulse), and (iii) the existence via Faraday rotation of relativistic electron currents accelerated in the forward direction during the laser pulse. Among other consequences, these results suggest the self-focusing of the laser pulse and a strong local heating of the plasma.

The experiments are performed with the P102 CPA laser system [1] at CEA/LV. A long creation laser pulse is focused by a $f/6$ lens through a random phase plate (RPP) onto a CH (polystyrene) foil (0.3 or 30 μm thick), 35° above the target normal. This 1.058 μm, 750 ps FWHM duration laser pulse has an average intensity of $3{-}5 \times 10^{12}$ W cm^{-2} (90% of 5 J is contained in a 400 μm focal spot). After a time delay, from 200 ps before to 1 ns after the maximum of the creation pulse, the subpicosecond frequency-doubled interaction beam at $\lambda =$ 529 nm is focused on the preformed plasma with a $f/3$ off-axis parabola at normal incidence and on the same side of the target as the creation beam. This 600 fs (FWHM) duration interaction beam has a maximum energy of 10 J, a 4×5 μm^2 focal spot (containing $\sim$20% of the laser energy), and a temporal contrast ratio better than 10^{12}:1 up to 30 ps before the maximum of the pulse. The remaining part of the energy is widely spread and does not contribute to the high intensity interaction. This leads to a maximum product intensity times the wavelength squared of $I\lambda^2 = 5 \times 10^{18}$ W cm^{-2} μm^2.

A diagnostic beam (0.35 μm wavelength, 1 ps pulse duration) is used to probe the plasma in the transverse direction 0 to 200 ps after the interaction beam. Using a Wollaston interferometer, this short pulse allows 2D, time-resolved density measurement of the preformed plasma and of the generated channel with a spatial resolution better than 5 μm [8]. The electron density is inferred by

 0031-9007/98/80(8)/1658(4)$15.00

Abel inversion of the interferograms. It is ramped from vacuum to densities well above the critical density. In the fully ionized underdense tail, the profile is approximated by a function $10^{-x/L}$, where x is the coordinate along the propagation axis. By varying the delay between the creation pulse and the interaction pulse as well as the thickness of the target it is possible to adjust the density scale length (L) in the 100–600 μm range. The maximum density that can be probed is around 4×10^{20} cm^{-3} for $L \sim 200$–300 μm. The refraction of the probe beam at higher densities produces the high-density dark area that can be seen at the right of Figs. 1 and 2. As a consequence, the evolution of the channel is hidden beyond this boundary. Faraday rotation measurements at $\lambda = 1.058$ μm from the unconverted part of the 1 ps probe beam are used to detect transverse self-generated magnetic fields.

Typical channel structures are shown in Figs. 1 and 2. At an intensity of $I\lambda^2 = 3 \times 10^{18}$ W cm^{-2} μm^2, for $L \sim 200$–300 μm, and 5 ps after the laser pulse has interacted with the target, a channel starting at low densities can be seen at the left of the interferogram in Fig. 1(a). On both Figs. 1 and 2 the laser vacuum focal spot lies on the target plane which is well off ($\sim$100 μm) on the right of the high-density dark area border. The polarization of the laser beam is linear and parallel to the surface of these images. The background density profile is shown in Fig. 1(b). The inferred radial density profile at a density of 10^{20} cm^{-3} [Fig. 1(c)] shows a maximum density perturbation of about -20% on axis. The profiles shown are the result of an averaging process involving a large number of fringes on both sides of the pointed fringe. For each fringe, we consider separately the top and bottom segments and their symmetric portion. For a slightly higher intensity ($I\lambda^2 = 4 \times 10^{18}$ W cm^{-2} μm^2) we observe at earlier time a nearly evacuated channel in its ending part as shown in Fig. 2. The radial density profile in the region of strong narrowing exhibits a -70% relative density perturbation on axis.

In steepened density profiles ($L \leq 100$ μm leading for the interferometry to a lower cutoff density $\sim 2 \times 10^{20}$ cm^{-3}) and at higher intensities ($I\lambda^2 \sim 5 \times 10^{18}$ W cm^{-2} μm^2), the channeling begins at higher densities ($\geq 10^{19}$ cm^{-3}) as diagnosed by interferometry. We then observe a transition from one channel to several density filaments as the density comes close to the 2×10^{20} cm^{-3} boundary. This could be the signature of beam breakup [4]. However, on some shots, we observe again a single and narrow (20 μm in diameter at 5 ps delay) channel in the denser regions. This transition could be the result of fluid outflow that fills up some filaments.

By varying the time delay between the interaction beam and the probe beam, we analyze the channel evolution at a density around 10^{20} cm^{-3} and for $L \sim 200$ μm. The radius of the channel for the first picoseconds of the evolution is shown in Fig. 3. From the slope of this curve, we measure an initial radial velocity of the expansion of 5×10^8 cm/s. Late time evolution ($\geq$100 ps) shows a drastic slowing of the expansion.

Another observation in these experiments is the presence of a large toroidal magnetic field along the propagation axis in the underdense plasma during and after the laser pulse. This can be seen in Fig. 4 in the case of a steep density profile ($L \sim 100$ μm) and during the laser pulse. The analyzer is rotated by 10° from extinction and the polarization rotation angle is deduced in the usual way [9] from the ratio between the signal and the background level. By measuring on the same shot the local electron density from the interferograms we deduce the amplitude of the magnetic field [9]. The maximum magnetic field amplitude deduced from Fig. 4 is located at a density near 10^{20} cm^{-3}. Several similar measurements made during

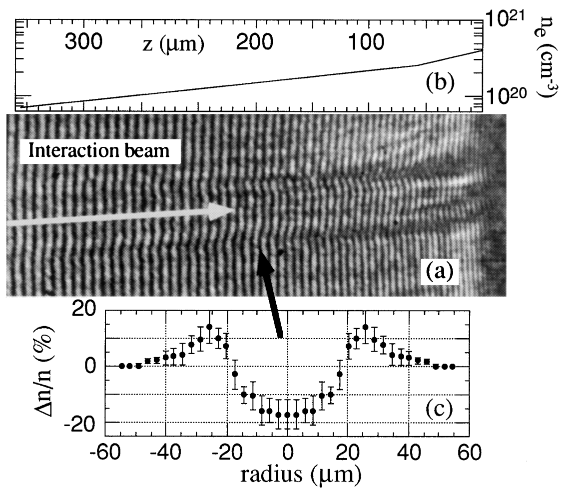

FIG. 1. (a) Interferogram showing the relativistic interaction beam channeling; (b) density profile along the propagation axis; (c) radial density profile extracted at a density $\sim 10^{20}$ cm^{-3}. Error bars in the radial density profile take into account uncertainties on the background density and the fringe pattern localization. The 3.3×10^{18} W cm^{-2} μm^2 interaction beam comes 500 ps after the creation beam on the 30 μm foil and the probe beam 5 ps after the interaction beam.

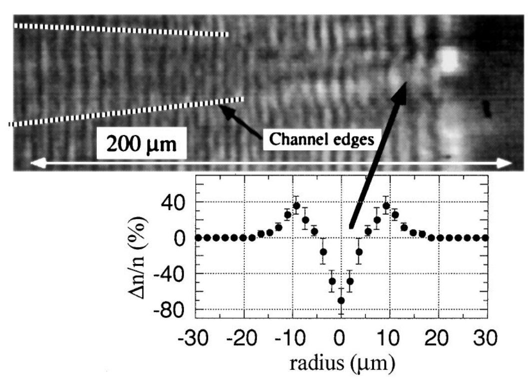

FIG. 2. Interferogram and radial density profile in the vicinity of a nearly evacuated channel. The 4.2×10^{18} W cm^{-2} μm^2 interaction beam comes 800 ps after the creation beam on the 30 μm foil and the probe beam 3 ps after the interaction beam.

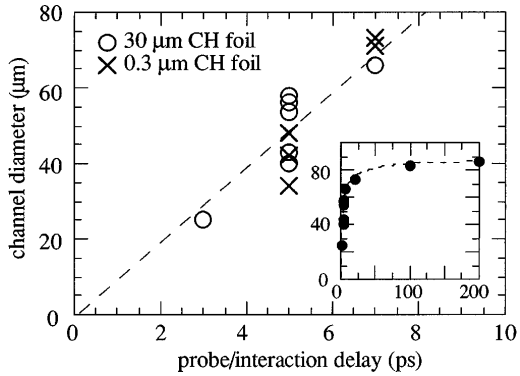

FIG. 3. Radial expansion of the channel edge as a function of the delay between the probe beam and the interaction beam. The slope gives a 5×10^8 cm/s expansion velocity. Inset: Late time evolution.

the laser pulse give a magnetic field amplitude between 70 and 35 MG. The polarigrams also show that the magnetic field decreases in the lower density part of the profile. Such a Faraday rotation has been observed only at full interaction beam intensity. The magnetic field amplitude is seen to decrease rapidly with a time constant ~ 3 ps. It is also worth noticing that the density at which the self-generated quasistatic magnetic field appears agrees well with the onset of the channel in the case of steepened profiles. Moreover, the maximum magnetic field amplitude is located where the channel is pinched and hollowed out.

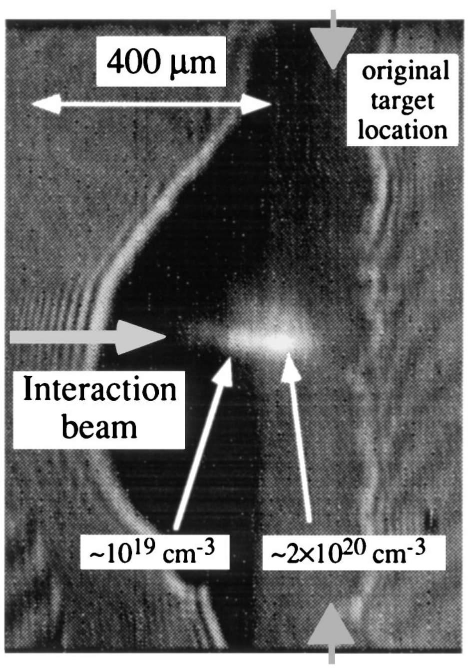

FIG. 4. Polarigram taken during the interaction of a 4.7×10^{18} W cm^{-2} μm^2 laser pulse with a heated 30 μm foil. The bright pattern is due to the polarization rotated probe beam under the effect of a 35 MG static magnetic field. The weak exposure is due to the leakage from the 10° rotation of the analyzer. All the beams (creation, interaction, and probe) are time coincidents.

Two-dimensional Cartesian PIC simulations have been performed with physical parameters close to the experimental conditions. The plasma density profile is a piecewise linear function ranging from $0.025 n_c$ up to $2 n_c$ fitting the experimental density of Fig. 1(b). This density is followed by a flat slab of density $2 n_c$ that models the overdense plasma of the experiment. The system size is approximately $460 k_0^{-1} \times 1650 k_0^{-1}$ ($36 \times 130\ \mu$m^2). There are 21 grid points per wavelengths ($dx = 0.3 k_0^{-1}$) and a total of about 160×10^6 particles. The time step is $0.28 \omega_0^{-1}$. The initial temperature of electrons is 4 keV. We verify that this choice, related to numerical stability reasons, is justified as, in the simulation, the interaction pulse heats in tens of fs the surroundings of the channel at a mean energy above 100 keV by parametric instabilities [10]. The laser beam is incident from the left and has a shape, intensity, and polarization (which is parallel to the surface of the images shown in Fig. 5) similar to the experimental one with a maximum amplitude corresponding to $I\lambda^2 = 5 \times 10^{18}$ W cm^{-2} μm^2. For economical reasons, the pulse length has been reduced by a factor of 2. This reduces the total energy by the same factor. Particles leaving a simulation box in the transverse direction or through the overdense plasma are absorbed and replaced

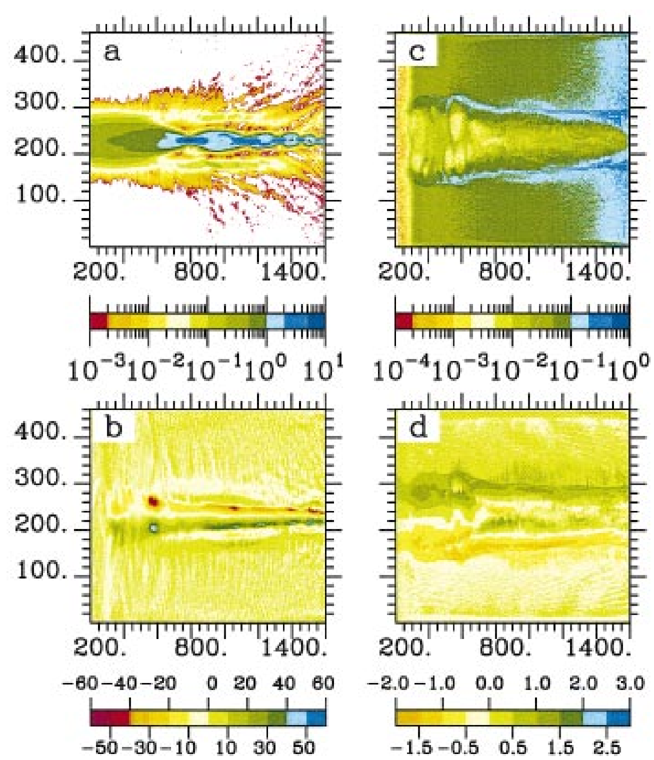

FIG. 5(color). Two-dimensional PIC Cartesian simulations in the same experimental conditions as in Fig. 1 (see text for simulation details). (a) Map of the laser Poynting vector value (scale is in fraction of its initial maximum), (b) quasistatic magnetic field map (scale is in Megagauss), (c) ion density map (scale is in fraction of n_c), and (d) ion expansion velocity map (scale is expressed in units of $10^{-2} c$). (a) and (b) are at the same time: 0.65 ps; (c) and (d) are at 1.25 ps.

by particles at the initial temperature. This avoids unphysical heating related to periodic boundary conditions in the transverse direction. The simulations were performed on 128 processors of a Cray/T3E.

Figure 5(a) shows the continuing self-focusing of the laser pulse at time 0.65 ps (i.e., when the maximum of the pulse is within the channel). At a density $\sim 10^{20}$ cm^{-3}, its diameter is reduced to ~ 2.5 μm (compared to the initial FWHM 5 μm diameter), and its intensity is increased by a factor of 10. For visibility the plots have been limited to $x = 1400 k_0^{-1}$ (corresponding approximately to $n = 0.2 \times n_c$). Figure 5(b) is a plot of the magnetic field as a function of space at the same time. The maximum magnetic field amplitude is in the range of 50 MG, in agreement with the experimental observation. Figures 5(c) and 5(d) are results at time 1.25 ps (i.e., the time at which the ending tail of the pulse has reached the right edge of the simulation box). Figure 5(c) is a plot of the ion density, the electron density (not shown) being the same. The late simulation time has been chosen for direct comparison with Fig. 1. The initial plasma edge is at $x = 100 k_0^{-1}$. The channel is clearly visible and significantly depleted by the laser pulse (the density is a few percent of n_c inside the channel). The edge density of the channel is almost constant and in the range $0.1 n_c$ to $0.2 n_c$. Figure 5(d) is a plot of the y component of the ion fluid velocity as a function of space. It clearly shows an expansion of the plasma edge with an approximate velocity in the range of $(3\text{–}4) \times 10^8$ cm/s. At that time plasma is seen to diffuse back inside the channel.

The physical mechanisms involved in the channel dynamics are the following. The radial ponderomotive force of the laser beam pushes the electrons out of the focal spot. However, the space-charge field maintains the quasineutrality between electrons and ions and accelerates the ions outwards [4]. They hollow out and expand the created density channel, as shown by the simulations and the interferometry. It should be emphasized here that at early times the PIC simulation shows that the ions move (along with the electrons) *during* the laser pulse. This enables the laser beam to focus inside this density depression and increase its intensity. As our laser power is about 40 times above the relativistic self-focusing threshold [5], we should also note that relativistic self-focusing can increase further the laser intensity. Self-focusing is supported by the fact that, both in the experiments and in the simulations, the observed magnetic field exhibits a flat and axially elongated shape that is quite different from what was seen in the experiments in the nanosecond regime [9]. This shape could be directly linked to a pipe-like shape of the fast electron current along the axial direction possibly generated by parametric instabilities [10,11]. The electron phase space projection given by the simulation evidences the anisotropy in the electron distribution function that is suggested by the magnetic field measurements. The late time transverse electron temperature is approximately 400 keV, whereas the energy distribution of the particles leaving the box on the right-hand side give an approximate temperature of 600 keV. Figure 1 can be understood in this self-focusing frame: We expect the ion velocity to be higher at higher densities (because the intensity is higher); this can overcome the difference in spot sizes (as the beam diameter is reduced at higher densities) and make the channel appear with an approximately constant diameter. On the contrary, Fig. 2 could be the result of filamentation that breaks the beam into filaments and strongly reduces the energy and diameter of the remaining filament that succeeds to stabilize. Thus the formed channel would appear with a smaller radius. At late times, as a result of the heating that occurs at early times, plasma diffuses back into the wide depleted channel. Indeed, the PIC simulation shows that, just after the laser pulse, ions are depleted below 1% of n_c inside the channel, whereas 5 ps later depletion is only of $\Delta n / n = -20\%$ as seen in Fig. 1(c).

In summary, we observe the formation of channels along the propagation axis of a relativistic subpicosecond laser pulse in a density-gradient underdense plasma. The plasma at the edge of the channel is accelerated to very large velocities (5×10^8 cm/s). Magnetic fields are observed with values around 50 MG during the laser pulse. These results suggest a self-channeling of the laser pulse in the plasma together with self-focusing and emission of a strong electron current along the axis. They are in good agreement with 2D PIC simulations. These experiments bring interesting results for the FI laser guiding scheme.

We would like to thank the P102-Castor staff at CEA Limeil for technical assistance and R. Caland for providing the targets. We wish also to thank T. W. Johnston, V. Malka, and A. Modena for fruitful discussions and R. Haroutunian for providing the Abel-inversion code. The PIC simulations were performed using IDRIS, the CNRS computer facility.

[1] N. Blanchot *et al.*, Opt. Lett. **20**, 395 (1995).
[2] M. Tabak *et al.*, Phys. Plasmas **1**, 1626 (1994).
[3] P. Young *et al.*, Phys. Rev. Lett. **75**, 1082 (1995), and references therein.
[4] W. Mori *et al.*, Phys. Rev. Lett. **60**, 1298 (1988).
[5] G. Mainfray and C. Manus, *Progress in Optics*, edited by E. Wolf (North-Holland, Amsterdam, 1993), Vol. 32, p. 313.
[6] A. Pukhov and J. Meyer-ter-Vehn, Phys. Rev. Lett. **76**, 3975 (1996).
[7] M. Borghesi *et al.*, Phys. Rev. Lett. **78**, 879 (1997).
[8] K. Bockasten, J. Opt. Soc. Am. **51**, 943 (1961); C. Vest, Appl. Opt. **14**, 1601 (1975).
[9] J. A. Stamper, Laser Part. Beams **9**, 841 (1991).
[10] J. C. Adam *et al.*, Phys. Rev. Lett. **78**, 4765 (1997).
[11] A. Modena *et al.*, Nature (London) **377**, 6 (1995); C. D. Decker *et al.*, Phys. Rev. E **50**, R3338 (1994); B. Quesnel *et al.*, Phys. Rev. Lett. **78**, 2132 (1997).